Validating LiDAR Sensor Surveillance Technology versus Conventional Out-the-window View for Safety-critical Airport Operations

Hannes Brassel, Alexander Zouhar and Hartmut Fricke
Chair of Air Transport Technology and Logistics
Technische Universität Dresden
Dresden, Germany
{hannes.brassel, alexander.zouhar, hartmut.fricke}@tu-dresden.de

***Abstract*— This paper performs a quantitative comparison between established surveillance techniques based on Out-The-Window View and Light Detection And Ranging (LiDAR) under identical visibility conditions. The aim is to understand how LiDAR technology can potentially improve the situational awareness of the Apron Air Traffic Controller (ATCo). Our work hereby extends previous evaluations of LiDAR technology with application to apron surveillance by explicitly comparing the visual performance of LiDAR and Out-The-Window View.**

ATCo scanning activities on the apron conceptually follow (a) object detection, (b) size estimation, (c) class recognition, and (d) identification, where "size" constitutes an essential distinctive visual feature. Hence, comparing different surveillance techniques can revert into judging the respective level of performance reached to solve these visual tasks per technology candidate. To that end, the presented quantitative comparison relies on performance indicators derived from a field experiment.

Our results show that LiDAR excels Out-The-Window View at degraded visibility conditions judged as the safety-critical setting. During good weather however, no winner can be identified specifically for the higher-level vision tasks (c) and (d). We so conclude, that LiDAR is a valuable candidate to significantly enhance the situational awareness of ATCo especially during adverse weather conditions and should be considered as a safety barrier.

Keywords*- *LiDAR, OTWV, airport ground surveillance, adverse weather, object detection, object size, class recognition, identification, LVO

I. Introduction

In today's Air Traffic Management (ATM) weather still constitutes a hardly predictable and uncontrollable, performance sensitive factor for both the Aircraft Operator (AO) and the Air Traffic Controller (ATCo). Especially, weather conditions have a significant safety performance impact on flight operations both en-route and on ground [1].

As for airport ground operations, still a large number of ATC procedures and advisories rely on line-of-sight conditions. Consequently, airport ground surveillance largely require Out-The-Window View (OTWV) capability for the ATCo. Dependent on local settings, the OTWV may be supported by e.g., video cameras (CCTV), Surface Movement Radar (SMR), secondary radar-based Multilateration (MLAT) and/or magnetic field sensors. As the OTWV directly links to the prevailing weather/lighting conditions such as e.g., fog during times of low visibility as defined in European Regulation (EU) No 965/2012 (IR-OPS Annex V Subpart E) for which ATC shall apply LVO. These operations however reduce significantly traffic throughput [2, 3]. The rationale of LVO and other such ATC measures is always to primarily grant the safety of flight operations at all times.

While the resulting capacity backlogs during LVO typically lead to economic losses (e.g. delays or network manager regulated traffic), a more critical case arises if a degraded ATCo's situational awareness would lead to a reduced ability to recognize conflicts and thus to poor decision making. This hazard was confirmed in several data studies such as in the Aviation Safety Reporting System (ASRS) analysis on ATCo-related safety-relevant occurrences, where 72.4% of all occurrences constituted in the failure to perceive information or are attributable to misperceived information [4]. According to IATA accident category distribution (2014-2018), over 10% of all aviation accidents in Europe result in ground damage, which is also in line with recent Boeing statistical summaries [5, 6]. The economic damage of a single ramp accident is estimated at $ 250,000 on average and $5 billion in total a year [7].

The International Civil Aviation Organization's (ICAO) concept for an Advanced Surface Movement Guidance and Control Systems (A-SMGCS) aims at overcoming the weather/lighting and line-of-sight dependencies of the OTWV in airport ground surveillance [8]. The most recent Eurocontrol Specification for A-SMGCS Services also considers automated controller assistance functions such as e.g., the detection of conflicts between aircraft or vehicles on or near the runway [9]. Light detection and Ranging (LiDAR) sensors combined with computer vision algorithms for object recognition seem to be a promising candidate for a cost-effective augmented reality solution compared to sole OTWV that functions well and that does not rely on cooperative objects to be controlled [10].

A. Problem statement and overview

Airport ground surveillance deeply relies on the real-time availability of highly precise and (weather/lighting) robust sensor data with high integrity and continuity levels capturing the local traffic situation on the movement area. It is therefore crucial to quantify to what extent the sensor-based performance equals the conventional one. To that end, this paper extends previous evaluations of LiDAR sensing (e.g. [11, 12, 13, 14, 15, 16]) through a quantitative comparison of established (OTWV) and LiDAR-based surveillance techniques under identical visibility conditions. We do aim to understand how LiDAR sensors can potentially improve the situational awareness of the ATCo as a crucial physiological safety metric. Most of the work in this direction has been done in the context of autonomous driving, however, emphasizing in this context on a performance comparison of LiDAR versus Radar/Camera [17].

ATCo scanning activities of the apron are streamlined by a set of visual tasks including (a) object detection (is there an object?), (b) object size estimation (how large is a detected object?), (c) class recognition a.k.a. classification (is the detected object an aircraft?) and (d) identification a.k.a. instance recognition (is the recognized aircraft an A320?). These tasks rely on increasingly detailed visual information of the scene in the sensory data by means of which the ATCo interprets the local traffic situation on the movement area. Hence, comparing different surveillance techniques can revert into judging the respective level of performance reached to solve these visual tasks per sensor candidate.

During a field experiment, selected probands (students) with domain knowledge on ATC procedures were asked to independently perform the previously described tasks (a)-(d) for a set of 23 test objects via OTWV and by examining a simultaneously recorded LiDAR image generated out of a so-called 3D point cloud capturing the same scene. The field experiments described in section II.A were conducted under four prevailing weather and lighting conditions: Clear/Day, Clear/Night, Rain/Day, and Rain/Night.

The recorded visibilities give rise to ”visual task scores” (section II.B) as performance indicators of the competing sensors (OTWV, LiDAR). This is in line with approaches presented in [18] where the visibility of static and moving objects on the airport surface was assessed in a remote tower control setting using the visual information captured by a camera system.

Next, section II.C addresses the quantitative comparison of the previously derived scores for OTWV and LiDAR recorded during the field experiments. Section III presents the experimental results and the validation of the performance criteria per sensor candidate and visual task based on the strategy outlined in section II.C. Finally, section IV concludes with a summary of the major findings and with an outlook on the next steps to be taken in this research.

B. Literature/Ongoing LiDAR Research

LiDAR is a laser-based method to determine distances between sensor and any object holding a reflective surface by measuring the travel time of the laser beam. Current LiDAR devices focusing on solid objects combine certain capabilities that excel conventional airport sensors: Non-cooperative environmental scanning, construction-related large angles of detection, high pulse repetition rates (PRR), signal transmission at pulse frequencies reaching petahertz range (≙ Extremely High Frequency, EHF) leading to an extraordinary precision and accuracy of position and pose at millimeter range level. State-of-the-art LiDAR sensors already cover well operationally relevant distances of up to several hundred meters, are eye-safe and do not suffer from ambiguous multipath effects. In contrast to environmental scanning using the spectrum of visible light (human eye, binoculars, video camera), LiDAR is considered as rather independent from light conditions (day/night) and less sensitive to weather conditions, however, more weather-sensitive than long-wave Radar, and others, SMR, MLAT [19, 20, 11, 21, 22].

Previous research has focused on LiDAR’s conceptual and practical capability of capturing the local traffic situation on the airport movement area, especially on the airport apron. In a preliminary experimental study [10], LiDAR’s precision and accuracy were assessed at the example of the detectable fuselage height changes due to loading of a parked Boeing 757-200 during the aircraft turnaround. Furthermore, computer vision algorithms were developed for LiDAR-based object recognition, e.g., in [23], focusing on the detection of small unknown static objects of a few cm² (Foreign Object Debris, FOD) on the apron. In [24], an algorithm was developed that successfully classified and estimated the poses of an Airbus A319-100 and a Boeing B737-700 parked at the gate. Motivated by these promising results, a comprehensive LiDAR-based surveillance concept for reducing risks in apron operations was developed in [25]. This concept was then experimentally assessed concerning its potential risk mitigation effects in [19]. Compared to conventional apron surveillance (OTWV, video cameras), it was shown that the ATCo’s hazard recognition rates increase by 18% on average whereas the reaction times decrease by 45% for an ideal LiDAR configuration.

C. Contribution

This paper proposes an experimental approach to quantitatively assess and compare the visual performance of LiDAR sensing technology and established airport ground surveillance techniques based on OTWV. Our approach hereby draws from previous work on camera-based surveillance techniques (CCTV) in remote tower control settings focusing on the expected visual performance of tower controllers [26].

The paper consists of three main contributions: (1) a generic field experiment where probands perform increasingly complex visual tasks (a)-(d) using OTWV and by examining a LiDAR image constructed out of a 3D point cloud recorded under identical visibility conditions, (2) the definition of visual task scores based on the recorded visibilities as performance indicators for the competing sensors (human, LiDAR), (3) a quantitative comparison of OTWV and LiDAR sensing under prevailing weather and lighting conditions as given during the field experiments. The results derived in this work shall help to better understand how the visual performance of LiDAR-based surveillance systems is compared to conventional techniques based on OTWV. Given such a comparison it is then possible to conclude if LiDAR is a valuable candidate to potentially improve the situational awareness of the ATCo as a crucial physiological safety metric and to potentially reduce the

Runway Visual Range (RVR) constraints for Low Visibility Procedures (LVP) thus increasing airport capacity while ensuring safe airport operations [27].

II. METHOD

In this section, we first describe the setup of the field experiments in order to assess the performance of the competing sensors (OTWV, LiDAR). Then, we will derive visual task scores as performance indicators of the sensors under four prevailing visibility conditions. Finally, we will address the quantitative comparison of the sensors using the previously derived scores.

A. *Data acquisition*

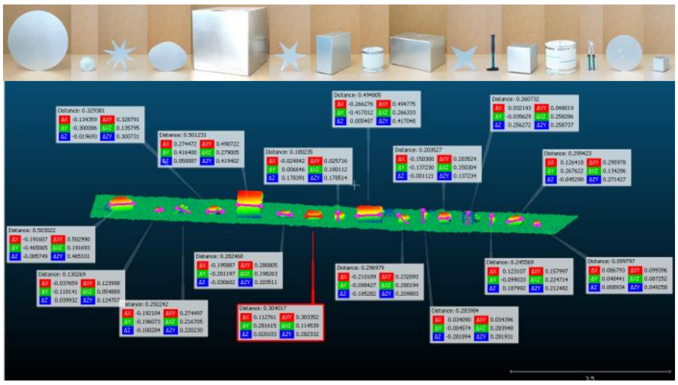

Figure 1. Shown are 16 out of 23 test objects (top row) and corresponding LiDAR point clouds scanned at 20 meters distance (second row) together with the object dimensions. Notice, that the object arrangement differs from the experimental setup depicted in Figure 3.

ATCo scanning activities of the apron are streamlined by a set of visual tasks carried out by highly normalized purpose trained humans, i.e., (a) object detection, (b) object size estimation, (c) class recognition a.k.a. classification and (d) identification a.k.a. instance recognition. These tasks rely on increasingly detailed visual cues of the scene in the sensory data by means of which the ATCo reasons about the local traffic situation on the movement area [28]. The performance of OTWV and LiDAR is therefore driven by the ability to resolve the visual cues associated with (a)-(d) under a variety of visibility conditions.

To that end, in this work, we propose the experimental setup shown in Fig. 3. The illustration depicts the sensor location together with the LiDAR scans of 23 test objects of varying sizes and shapes arranged at fixed locations relative to the sensor (see also Fig. 1). The test objects were placed on a concrete-like ground surface and consist of metallic surfaces with similar reflectance properties of objects typically appearing on the apron (e.g. cars, buses, aircraft, ground personnel wearing a reflective vest, tools). Notice, that the test objects were arranged such that their sizes give rise to roughly evenly distributed angular diameters ranging from 2 to 90 arcmin. Fig. 2 illustrates how the angular diameter of some typical objects evolves as a function of the relative distance from the sensor where the object size was used as foundation of the angular diameter range. The angular diameter of 8 arcmin, for example, may resemble a FOD with a size of 10 cm located on the apron with a relative distance of approximately 50 m to the sensor.

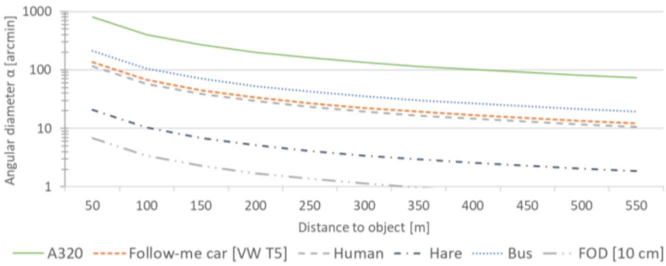

Figure 2. Angular diameters of exemplary objects as a function of the relative distance between sensor and object.

Ideally, the limiting resolution of the imaging/sensor system should at least be equivalent to the ATCo's ability to perceive a given detail. From human factors research [29, p. 401] it is known that humans can theoretically reach a visual acuity of approximately one arcmin [′], where

$$1° = 60 \text{ arcmin } [′], \alpha = 2 \arctan\left(\frac{g}{2r}\right) \cdot 60[′]. \quad (1)$$

In (1) the quantities α, g and r denote the angular object diameter [′], the object size (often measured in meter [m]) and the distance of an object from the sensor (also measured in meter [m]), respectively. However, in reality and specifically under non-ideal visibility conditions it is reasonable to assume that the minimum achievable acuity is not less than 2 arcmin [18, p. 64].

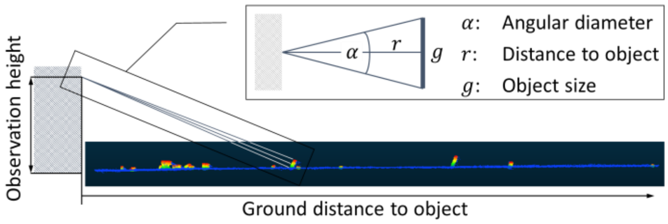

Figure 3. Illustration of the experimental setup. Shown is a side view of the LiDAR point clouds capturing the test objects. The line of sight distance, ground distance and the object size give rise to the angular object size according to (1).

As noted in section I.A, the complexity of the visual tasks (a)-(d) increases with the level of detail that a sensor is required to resolve. This granularity of visual recognition gives rise to the expected outcome of the visual tasks for the test objects in TABLE I. The selection of the test objects was motivated by the recognition following the components-theory [30] in which various characteristic parts of a visual scenery are used separately to determine if and where an object of interest exists. For example, the objects depicted in the top row in Fig. 4 may be recognized based on their 2D/3D shape primitives shown in the second row in Fig. 4 including circles, cylinders, cuboids, stars, and others. Hence, the test objects resemble a variety of characteristic 2D/3D shapes that appear on the apron either as (projected) components of larger objects (e.g. the front view of aircraft stabilizers resembles a star) or as entire objects (e.g. a toolbox looks like a cuboid).

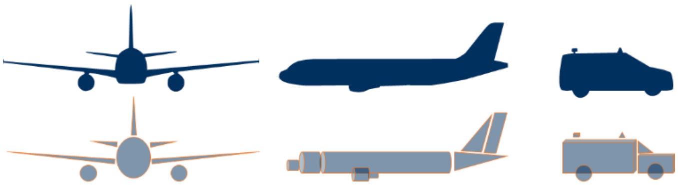

Figure 4. Recognition by components. Possible compositions of the objects shown in the first row are highlighted in the second row.

As noted above, the expected outcome of the visual tasks in TABLE I dictates the level of detail the sensor needs to resolve.

Object detection, for example, reduces the visual task to a binary decision indicating if an object is visible or not. Size estimation (largest object dimension) involves the perception of object boundaries and the notion of distance. Object size is an important visual cue that is often used in point-based recognition where a LiDAR sensor is used to achieve a high degree of robustness against adverse weather/lighting conditions [31, 16]. Class recognition, on the other hand, involves a coarse, global description of the shape, such as angular/star, round or elongated. Finally, at the level of identification, the distinction between the shapes derives from fine-grained details, such as spherical or elliptical, square/cube or rectangle/cuboid, how many spikes a star has and others.

TABLE I. VISUAL TASKS AND EXPECTED OUTCOMES.

Object: length (l)/width (w)/height (h) or diameter (Ø) [cm]		**Object-specific visual task**			
		Detection	***Size Estimation***	***Class recognition***	***Identification***
	1: *3/3/-* 2: *4,5/4/-* 3: *4,8/3,5/-* 4: *8,8/6,5/-* 5: *59/16/-* 6: *77/16/-*	Yes/No	max(l/w)	Angular object	Flat rectangle
	7: *30/50/30* 8: *15/30/30*	Yes/No	max(l/w/h)		3D cuboid
	9: *10/10/10* 10: *20/20/20* 11: *50/50/50*	Yes/No			3D cube
	12: *Ø 12* 13: *Ø 30* 14: *Ø 50*	Yes/No	Ø	Round object	Flat round slice
	15: *25/32/-*	Yes/No	max(l,w)		Flat ellipse
	16: *-/-/23; Ø 26* 17: *-/-/17; Ø 18*	Yes/No	max(h, Ø)		3D circular cylinder
	18: *Ø 30* (Four spikes) 19: *Ø 29* (Six spikes) 20: *Ø 30* (Eight spikes)	Yes/No	Ø	Star shape	Star with indication of the number of spikes
	21: *5,5/25/1,5* (Pipe wrench) 22: *2,5/30/10* (Hammer)	Yes/No	max(l/w/h)	Elongated object	21: Pipe wrench 22: Hammer
	23: *36/12/23* (Toolbox)	Yes/No		Angular object	Toolbox/ Suitcase

Besides the configuration of the test objects, the visibility conditions are a key limiting factor affecting the sensor performance. To consider this fact, we acquired sensor data (OTWV, LiDAR) under four different weather/lighting conditions according to the ICAO specification of common weather phenomena that reduce visibility [32]. TABLE II summarizes the visibility specific test scenarios together with the corresponding ICAO visibility classes.

TABLE II. VISIBILITY SCENARIOS (ICAO DOC. 9328 AN/908) [32] DURING THE FIELD EXPERIMENTS.

Visibility Scenario	**Description**
Clear/Day:	Clouds and visibility okay (CAVOK) according to Meteorological Terminal Air Report (METAR) during daytime.
Clear/Night:	CAVOK during nighttime.
Rain/Day:	"Precipitation in the form of liquid water drops, varying in size from 0.5 to a maximum of 6 mm in diameter […]" [32] during daytime.
Rain/Night	Rain during nighttime.

Given the setup in Fig. 3, about 150 probands were asked to perform the visual tasks summarized in TABLE I. For a particular visibility scenario in TABLE II, one half of the test persons examined the scene independently from using OTWV. The per-object responses were recorded and passed to the subsequent validation in Section III. Moreover, the scenery was scanned simultaneously using the LiDAR sensor thereby ensuring equivalent visibility conditions. Then, the second group of test persons (different from the first group) conducted the vision experiments in TABLE I by examining the corresponding LiDAR scans using a visualization software (e.g. CloudCompare [33]). The per-object findings were again documented and passed on to validation. For each visual task, we recorded at least 10 responses per object to collect a statistically significant number of outcomes.

The procedure described above was repeated for all visibility scenarios in TABLE II. We would like to note here that all of the selected probands (students) have domain knowledge on ATC procedures. Moreover, the test persons were instructed to inspect the scene without visual aids such as binoculars by looking out the open window without the influence of reflections and the filtering effects arising at shaded windowpanes. Also note, that the night vision scenarios in TABLE II were partially influenced by ambient light sources, such as street lights.

The LiDAR sensor at our disposal is a first-generation OPAL 360 HP sensor developed by Neptec. The sensor provides a horizontal field of view of 360° and a vertical field of view of 45° with an azimuthal resolution of 0.0057°, which exceeds the visual acuity of human eyes by a factor of three. The level of detail captured by the sensor, however, greatly depends on the Pulse Repetition Rate (PRR) and the scanning duration building the point cloud. The latter may be derived from the time between subsequent movements for smaller airports (arrivals/departures) in which the apron controller can resolve potential incidents on the airfield. Assuming a scanning duration of 2 min and a PRR of 200 kHz, the LiDAR sensor forms a cloud comprising of up to 24 million points (x, y, z, timestamp, intensity) (see Fig. 1 and Fig. 3).

B. Definition of visual task scores

In this section, we quantify the performance of the candidate sensors per visual task setting described in Section II.A. The values of the derived quantities are referred to as *scores* to indicate that larger values are better.

The size estimation score for a known target object, denoted S_g may readily be defined in terms of (2) where the quantity $S_g \in [0\%, 100\%]$ is a function of the estimated object size given the true size g. Size estimates $\hat{g}$ with $\hat{g} \geq 2g$ are treated as outliers and are mapped to $S_g = 0$.

The scores for visual detection, class recognition, and identification derived from the frequency distribution of correct outcomes of the vision experiments per target object in TABLE III. Let $T > 0$ denote the number of test persons, then the scores S_D, S_R, $S_I \in [0\%, 100\%]$ in (2) - (5) should read respectively as predicted probabilities of visual detection, class recognition and identification per target object where the quantities N_D, N_R, N_I are the frequencies of correct outcomes of the associated vision experiments. Similar quantities were devised by the Federal Aviation Agency (FAA) to assess the visual performance of ATCo's, thereby emphasizing on OTWV to facilitate the design of new towers [34].

TABLE III. VISUAL TASK SCORES. LARGER VALUES ARE BETTER.

Visual task	Score function for a single target object
Size estimation	$S_g = \max\left(0; 1 - \frac{\lvert g - \hat{g}\rvert}{g}\right) \cdot 100\ [\%]$ (2)
Detection	$S_D = \frac{N_D}{T} \cdot 100\ [\%]$ (3)
Class recognition	$S_R = \frac{N_R}{T} \cdot 100\ [\%]$ (4)
Identification	$S_I = \frac{N_I}{T} \cdot 100\ [\%]$ (5)

C. Quantitative comparison of OTWV and LiDAR

In this section, we outline our strategy to quantitatively compare the visual performance of the competing sensors. Such a comparison helps to find out how LiDAR sensors can potentially improve the situational awareness of the ATCo. To this end, it is essential to provide performance indicators of the sensors. The latter may readily be derived from the previously defined scores (2) - (5) by noting that the central tendency of the scores is governed by the average or expected value of the scores. Hence, for a particular visibility scenario in TABLE II the sensor with the highest score tends to perform better.

For example, assuming that the visual task score under consideration is required to lay within some range then the expected scores (e.g., a detection score of 90% [35]) give rise to angular diameters that the sensor is able to resolve.

In addition to expressing the expected value, the standard deviation quantifies the amount of variation of the scores as a function of the angular diameter. Larger deviations, for example, indicate a higher degree of uncertainty suggesting that the underlying sensor measurements tend to be less reliable. Notice, that without further knowledge about the shape of the underlying distribution of the score data we shall assume that the scores are drawn independently from a Gaussian distribution whose mean and variance are unknown.

III. RESULTS

In this section, we validate the outcome of the field experiments described in section II. To that end, the measurements were processed based on the visibility scenarios in TABLE II.

Specifically, the day- and night-time scenarios indicate how changing luminance influences the performance of OTWV and LiDAR [36, 37, 38], whereas the clear and rain scenarios give rise to different wavelength-dependent extinction coefficients affecting the attenuation of the sensor signal passing through the atmosphere [39, 40, 36]. In addition, the proportion of the returned radiation energy density is largely affected by the wavelength-dependent reflectance of the test objects which in our case constitute (ideal) metallic surfaces [41].

Given the object-specific scores (2) - (5) we estimate the expected values and standard deviations of the scores as performance indicators of OTWV and LiDAR where we make the simplifying assumption that the observed scores are normally distributed. The estimates were obtained by using an average smoothing kernel with a window width of 10 arcmin centered at discrete intervals in the angular diameter range. For simplicity, the remaining values of the predicted score functions were linearly interpolated between the expected scores. As a result, each visibility scenario in TABLE II gives rise to the regression curves and the associated standard deviations in Fig. 5 – Fig. 8 indicating the sensor performance for each visual task.

Overall, the figure plots suggest that LiDAR outperforms OTWV especially in the night-time scenarios in Fig. 6 and Fig. 8. The latter is due to the well-known fact that the human acuity of vision decreases with diminishing illumination [42].

An important observation is that LiDAR achieves an expected detection score of almost 100% across all visibility scenarios. Similar to detection, LiDAR also reaches higher scores and lower standard deviations than OTWV when it comes to size estimation indicating that in this case, human perception is less reliable and largely dependent on the scene context. Notice, that a score of zero corresponds to failed detections or overestimations according to (2). Significant deviations from this trend can be seen for the higher-level vision tasks (class recognition, identification) in Fig. 5 and Fig. 7 where the daylight conditions seem to benefit OTWV in terms of additional color/contrast information.

Notice, that both for OTWV and LiDAR decreasing scores are typically accompanied by higher uncertainties (standard deviations) across all scenarios. This is not surprising due to the limited ability of OTWV and LiDAR to resolve details especially when it comes to smaller, complex shapes (e.g., tools and star-like shapes). On the other hand, the standard deviations of OTWV are larger across all scenarios compared to LiDAR confirming that LiDAR operates with higher precision than OTWV.

Also notice, how the changing illumination from day-time in Fig. 5 and Fig. 7 to night-time in Fig. 6 and Fig. 8 reduces the performance of OTWV even for the higher-level vision tasks compared to LiDAR confirming that human vision is susceptible to luminance.

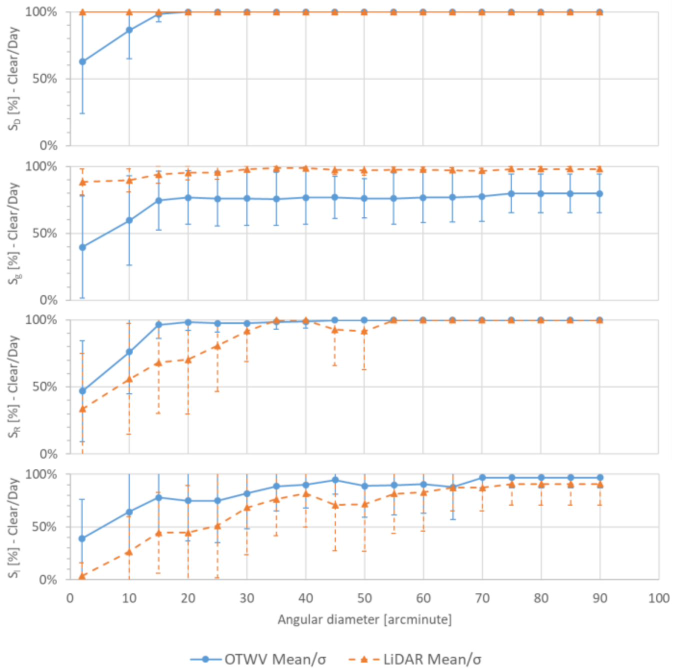

Figure 5. Expected visual task scores and standard deviations σ (standard error bars) for OTWV (blue) and LiDAR (red) for the scenario **Clear/Day**.

TABLE IV. RESOLVABLE ANGULAR DIAMETER AT 90% SCORE FOR THE SCENARIO **CLEAR/DAY**

Visibility Scenario	Description	
	OTWV	*LiDAR*
Clear/ Day	$\alpha(S_D = 90\%) \approx 12'$	$S_D = 100\%^a$
	$S_{g_{max}} = 80\%$ at $\alpha = 75'$	$\alpha(S_g = 90\%) = 10'$
	$\alpha(S_R = 90\%) = 13'$	$\alpha(S_R = 90\%) = 29'$
	$\alpha(S_I = 90\%) = 40'$	$\alpha(S_I = 90\%) = 76'$

a. For all objects and distances

The examples in TABLE IV compactly illustrate the visual performance of OTWV and LiDAR based on Fig. 5 by computing the angular diameters that the sensors are able to resolve at a visual task score of 90%. While the detection score of OTWV drops significantly compared to LiDAR as soon as the angular diameter decreases below a value of 15 arcmin, OTWV resolves object classes and instances better than LiDAR. By comparison, the example in TABLE V illustrates that LiDAR performs slightly better than OTWV considering the clear/night scenario in Fig. 6. Assuming a minimum achievable score of 90% the minimum resolvable angular diameter for OTWV increases especially for class recognition and identification due to the fact that smaller, more complex shapes are harder to recognize and to identify.

Likewise, the example in TABLE VI presents the minimum resolvable angular diameter at an achievable score of 90% for the scenario rain/day in Fig. 7.

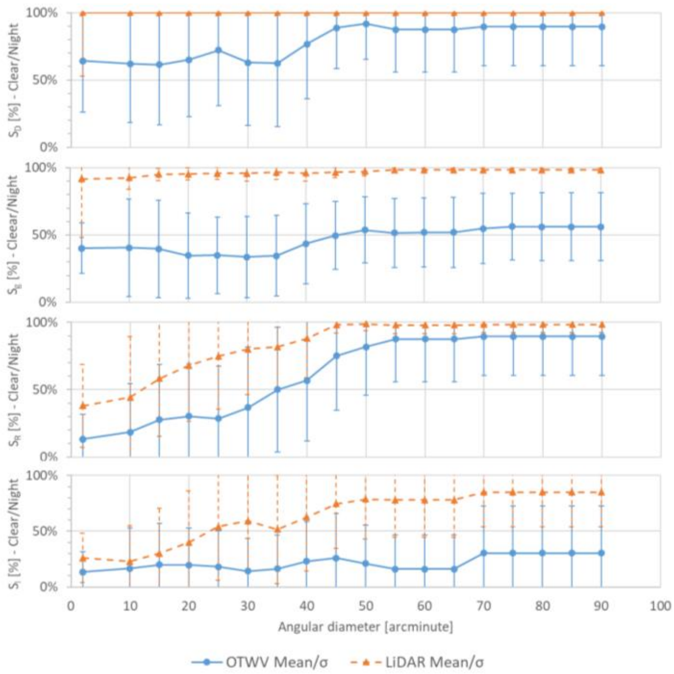

Figure 6. Expected visual task scores and standard deviations σ (standard error bars) for OTWV (blue) and LiDAR (red) for the scenario **Clear/Night**.

TABLE V. RESOLVABLE ANGULAR DIAMETER AT 90% SCORE FOR THE SCENARIO **CLEAR/NIGHT**

Visibility Scenario	Description	
	OTWV	*LiDAR*
Clear/ Night	$\alpha(S_D = 90\%) = 47'$	$S_D = 100\%^a$
	$S_{g_{max}} = 56\%$ at $\alpha = 75'$	$S_g \geq 92\%^a$
	$S_{R_{max}} = 89{,}58\%$ at $\alpha = 70'$	$\alpha(S_R = 90\%) = 41'$
	$S_{I_{max}} = 30\%$ at $\alpha = 70'$	$S_{I_{max}} = 85\%$ at $\alpha = 70'$

a. For all objects and distances

Similar to the clear/day example in TABLE IV, the minimum resolvable angular diameter of OTWV tends to be smaller or similar for classes recognition and identification compared to LiDAR. The notable performance gain of OTWV in the case of identification in TABLE VI compared to TABLE IV was most likely caused by the absence of shadows and glare induced by sunlight. However, we believe, that increasingly challenging visibility conditions due to heavy rainfall and fog will consistently reduce the performance of OTWV compared to LiDAR.

Finally, the example in TABLE VII confirms the trend of the visual task scores under the night/rain conditions depicted in Fig. 8 where LiDAR outperforms OTWV in all tasks on average. Similar to the scenario clear/night in Fig. 6 and the example in TABLE V one can see the dominating effect of luminance on OTWV compared to LiDAR.

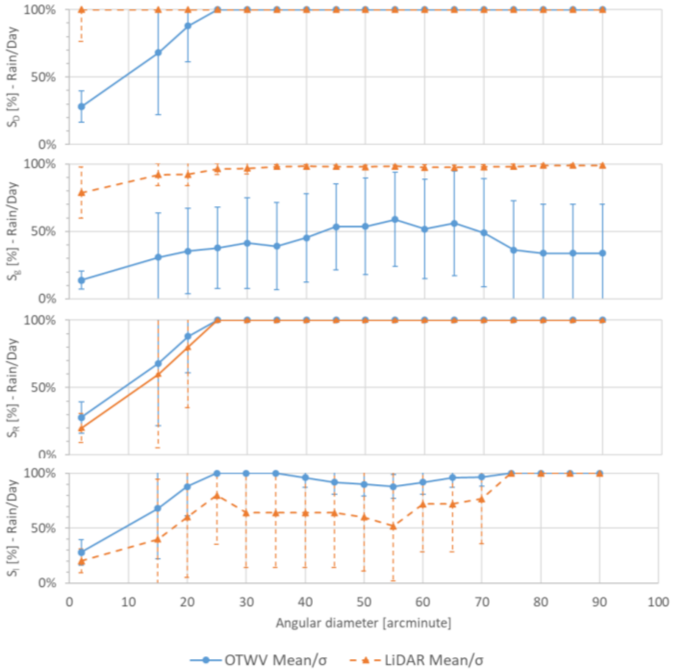

Figure 7. Expected visual task scores and standard deviations σ (standard error bars) for OTWV (blue) and LiDAR (red) for the scenario **Rain/Day**.

TABLE VI. RESOLVABLE ANGULAR DIAMETER AT 90% SCORE FOR THE SCENARIO **RAIN/DAY**

Visibility Scenario	**Description**	
	OTWV	***LiDAR***
Rain/ Day	$\alpha(S_D = 90\%) = 21'$	$S_D = 100\%^a$
	$S_{g_{max}} = 59\%$ at $\alpha = 55'$	$\alpha(S_g = 90\%) = 14'$
	$\alpha(S_R = 90\%) = 21'$	$\alpha(S_R = 90\%) = 23'$
	$\alpha(S_I = 90\%) = 21'$	$\alpha(S_I = 90\%) = 73'$

a. For all objects and distances

IV. CONCLUSION AND OUTLOOK

This paper presented a quantitative comparison of OTWV and LiDAR to better understand how LiDAR sensors can potentially improve the situational awareness of ATCo's. To this end we defined two performance indicators and provided experimental data of visual tasks under four prevailing visibility conditions. Our key findings are that LiDAR performs similar to OTWV in the daytime scenarios whereas during nighttime LiDAR consistently outperforms OTWV. Moreover, in all visibility scenarios, LiDAR exhibits a higher degree of accuracy than OTWV for object detection and size estimation while at the same time inducing less uncertainty in the sensor measurements. In view of automated workflows in apron surveillance we believe that LiDAR sensors are well suited to complement established procedures based on OTWV thereby augmenting the situational awareness of ATCo's.

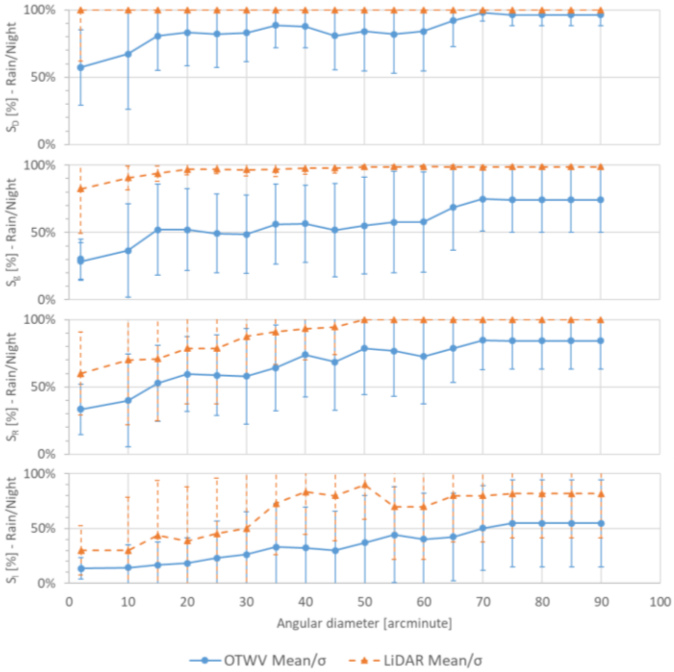

Figure 8. Expected visual task scores and standard deviations σ (standard error bars) for OTWV (blue) and LiDAR (red) for the scenario **Rain/Night**.

TABLE VII. TABLE I. RESOLVABLE ANGULAR DIAMETER AT 90% SCORE FOR THE SCENARIO **RAIN/NIGHT**

Visibility Scenario	***Description***	
	OTWV	***LiDAR***
Rain/ Night	$\alpha(S_D = 90\%) = 64'$	$S_D = 100\%^a$
	$S_{g_{max}} = 74\%$ at $\alpha = 70'$	$\alpha(S_g = 90\%) = 10'$
	$S_{R_{max}} = 85\%$ at $\alpha = 70'$	$\alpha(S_R = 90\%) = 34'$
	$S_{I_{max}} = 55\%$ at $\alpha = 75'$	$\alpha(S_I = 90\%) = 50'$

a. For all objects and distances

Along those lines, our future work continues to address the development of computer vision (CV) algorithms to automatically detect, recognize and identify objects of interest in LiDAR point sets capturing the apron especially under challenging weather and lighting conditions. Solving these visual tasks automatically is a crucial prerequisite for the design of automatic controller assistance functions such as the detection of conflicts between aircraft or vehicles on the movement area in real-time. At the same time the solution of visual tasks in unordered point sets is an extremely challenging topic in CV research. The results presented in this paper also serve as a prerequisite to examine the relationship between the spatial arrangement of multiple LiDAR sensors covering a certain range of the movement area and the profitability requirements of the resulting LiDAR system.

References

[1] Eurocontrol, "Performance Review Report," Brussel, 2018.

[2] M. Schultz, S. Lorenz, R. Schmitz and L. Delgado, "Weather Impact on Airport Performance," MDPI, Basel, 2018.

[3] M. Hakkeling-Mesland, B. van Beek, F. Bussink, M. Mulder and M. van Paassen, "Evaluation of an Autonomous Taxi Solution for Airport Operations during Low Visibility Conditions," Ninth USA/Europe Air Traffic Management Research and Development Seminar, 2011.

[4] D. Jones and M. Endsley, "Sources of Situation Awareness Error," Aviation, Space and Env. Medicine, 1996.

[5] IATA, "Safety Report 2018 (Issued April 2019), 55th Edition," Montreal, 2019.

[6] BOEING, "Statistical Summary of Commercial Jet Airplane AccidentsWorldwide Operations | 1959 – 2017," Seattle, 2018.

[7] M. Lacagnina, "Defusing the Ramp," Flight Safety Foundation, 2007.

[8] ICAO, "Advanced SurfaceMovement Guidanceand Control Systems(A-SMGCS) Manual Doc 9830," Montreal, 2004.

[9] Eurocontrol, "Specification for A-SMGCS," Brussel, 2018.

[10] L. Meyer, J. Mund, B. Marek and H. Fricke, "Performance test of LiDAR point cloud data for the support of apron control services," ESAVS, Berlin, 2013.

[11] M. Kusenbach, M. Himmelsbach and H.-J. Wünsche, "A New Geometric 3D LiDAR Feature for Model Creation and Classification of Moving Objects," IEEE Intelligent Vehicles Symposium (IV), 2016.

[12] P. Radecki, M. Campbell and K. Matzen, "All Weather Perception: Joint Data Association, Tracking, and Classification for Autonomous Ground Vehicles," Computer Research Repository, 2016.

[13] A. Börcs, B. Nagy and C. Benedek, "Instant Object Detection in Lidar Point Clouds," IEEE Geoscience and Remote Sensing Letters, vol. 14, no. 7, 2017, pp. 992-996.

[14] M. Bijelic, T. Gruber and W. Ritter, "A Benchmark for Lidar Sensors in Fog: Is Detection Breaking Down?," IEEE Intelligent Vehicles Symposium, Changshu, Suzhou, China, 2018.

[15] C. Goodin, D. Carruth, M. Doude and C. Hudson, "Predicting the Influence of Rain on LIDAR in ADAS," MDPI electronics, Mississippi State, 2019.

[16] J. Mund, A. Zouhar and H. Fricke, "Performance Analysis of a LiDAR System for Comprehensive Airport Ground Surveillance under Varying Weather and Lighting Conditions," ICRAT, Castelldefels, 2018.

[17] S. Zang, M. Ding, D. Smith, P. Tyler, T. Rakotoarivelo and M. A. Kaafar, "THE IMPACT OF ADVERSE WEATHER CONDITIONS ON AUTONOMOUS VEHICLES," IEEE, 2019.

[18] N. Fürstenau, Virtual and Remote Control Tower, Switzerland: Springer, 2016.

[19] J. Mund, P. Latzel and H. Fricke, "Can LiDAR Point Clouds effectively contribute to Safer Apron Operations?," Proceedings of the 6th SID, Delft, 2016.

[20] Z. Koppanyi and C. Toth, "Estimating aircraft heading based on laserscanner derived point clouds," ISPRS Annals of the Photogrammetry, Remote Sensing and Spatial Information Sciences, München, 2015.

[21] Z. Koppanyi, C. K. Toth and S. Young, "Centerline Deviation Estimation from Point Clouds using LiDAR Imagery," 7th International Conference on Research in Air Transportation (ICRAT 2016), Philadelphia, 2016.

[22] R. Rasshofer and K. Gressner, "Automotive radar and lidar systems for next generation driver assistance functions," in *ARS*, 2005, pp. 205-209.

[23] J. Mund, A. Zouhar, L. Meyer, H. Fricke and C. Rother, "Performance Evaluation of LiDAR Point Clouds towards Automated FOD Detection on Airport Apron," Proceedings of the 5th International Conference on Application and Theory of Automation in Command and Control Systems (ATACCS), Toulouse, 2015.

[24] J. Mund, F. Michel, F. Dieke-Meier, H. Fricke and L. Meyer, "Introducing LiDAR Point Cloud-based Object Classification towards Safer Apron Operations," Proceedings of the International Symposium on Enhanced Solutions for Aircraft and Vehicle Surveillance Applications, Berlin, 2016.

[25] J. Mund, L. Meyer and H. Fricke, "LiDAR Performance Requirements and Optimized Sensor Positioning for Point Cloud-based Risk Mitigation at Airport Aprons," Proceedings of the 6th International Conference on Research in Air Transportation, Istanbul, 2014.

[26] W. Krebs, G. Hewitt, S. Murrill and R. Driggers, "How high is high enough? Quantifying the impact of air traffic control tower observation height on distance perception.," in *Proceedings of the 13th Annual International Symposium on Aviation Psychology*, 2005, pp. 322-326.

[27] ICAO, "Manual of All-Weather Operations Doc 9365AN/910," Montreal, 2013.

[28] K. O. Johnson and J. R. Phillips, "Johnsons criteria: Tactile spatial resolution. I. Two-point discrimination, gap detection, grating resolution, and letter recognition," in *American Physiological Society*, 1981, pp. 1177-1192.

[29] D. Malacara-Hernández and Z. Malacara-Hernández, Handbook of Optical Design, CRC Press, 2017.

[30] I. Biederman, "Recognition-by-components: A theory of human image understanding.," in *Psychological Review, Vol 94(2)*, Washington, American Psychological Association, 1987, pp. 115-147.

[31] M. Jokela, M. Kutila and P. Pyykönen, "Testing and Validation of Automotive Point-Cloud Sensors in AdverseWeather Conditions," MDPI applied sciences, Finland, 2019.

[32] ICAO, "Manual of Runway Visual Range Observing andReporting Practices Doc 9328," Montreal, 2005.

[33] "CloudCompare 3D point cloud and mesh processing software," [Online]. Available: http://www.cloudcompare.org/. [Accessed 04 09 2019].

[34] FAA, "Federal Aviation Administration," U.S. Department of Transportation, 2017. [Online]. Available: https://www.hf.faa.gov/visibility/. [Accessed 04 09 2019].

[35] FAA, "Airport Foreign Object Debris (FOD) Detection Equipment; AC No:150/5220-24," Washington, D.C., 2009.

[36] M. N. Favorskaya and L. C. Jain, Handbook on Advances in Remote Sensing and Geographic Information Systems: Paradigms and Applications in Forest Landscape Modeling, 2017: Springer.

[37] FAA, "Air Traffic Control Visibility Analysis Tool," [Online]. Available: https://www.hf.faa.gov/visibility/help.aspx. [Accessed 11 09 2019].

[38] D. Brunt, Physical and Dynamical Meteorology, Cambridge: Cambridge University Press, 2011.

[39] J. Wojtanowski, M. Kaszczuk, M. Zygmunt and M. Muzal, "Comparison of 905 nm and 1550 nm semiconductor laser rangefinders' performance deterioration due to adverse environmental conditions," Versita, Warszawa, 2014.

[40] A. Bennett, "Introduction to atmospheric visibility estimation," Biral, Bristol, 2012.

[41] F. Incropera, D. DeWitt, T. Bergmann and A. Lavine, Fundamentals of heat and mass transfer, Hoboken: John Wiley & Sons, 2011.

[42] H. Davson, The Visual Process, London: Elsevier Inc., 1962.

[43] EUROCAE, "Minimum Aviation System Performance Specification for Advanced Surface Movement Guidance and Control Systems (A-SMGCS) Levels 1 and 2," 2015.

[44] M. Hebel, M. Arens and U. Stilla, "Change detection in urban areas by object-based analysis and on-the-fly comparison of multi-view ALS data," ISPRS Journal of Photogrammetry and Remote Sensing Volume 86, 2013, pp. 52-64.

[45] WMO, "Chapter 9 - Measurement of visibility," in *Measurement of meteorological variables*, Genf, World Meteorological Organization (WMO), 2014, p. 294.

[46] C. Van Daalen, "Conflict Detection and Resolution for Autonomous Vehicles," 2010.